arXiv:1411.4198v3 [cond-mat.mtrl-sci] 18 Mar 2016

Shock-waves and commutation speed of memristors

Shao Tang,[1] Federico Tesler,[2] Fernando Gomez Marlasca,[3] Pablo Levy,[3] V. Dobrosavljević,[1] and Marcelo Rozenberg[4]

[1]*Department of Physics and National High Magnetic Field Laboratory, Florida State University, Tallahassee, FL 32306, USA*

[2]*Departamento de Física - IFIBA, FCEN, Universidad de Buenos Aires, Ciudad Universitaria Pabellón I, (1428) Buenos Aires, Argentina*

[3]*GIA-CAC - CNEA, Av. Gral Paz 1499 (1650) San Martín, Pcia Buenos Aires, Argentina.*

[4]*Laboratoire de Physique des Solides, CNRS-UMR8502, Université de Paris-Sud, Orsay 91405, France*

Progress of silicon based technology is nearing its physical limit, as minimum feature size of components is reaching a mere 10 nm. The resistive switching behaviour of transition metal oxides and the associated memristor device is emerging as a competitive technology for next generation electronics. Significant progress has already been made in the past decade and devices are beginning to hit the market; however, it has been mainly the result of empirical trial and error. Hence, gaining theoretical insight is of essence. In the present work we report the striking result of a connection between the resistive switching and *shock wave* formation, a classic topic of non-linear dynamics. We argue that the profile of oxygen vacancies that migrate during the commutation forms a shock wave that propagates through a highly resistive region of the device. We validate the scenario by means of model simulations and experiments in a manganese-oxide based memristor device. The shock wave scenario brings unprecedented physical insight and enables to rationalize the process of oxygen-vacancy-driven resistive change with direct implications for a key technological aspect – the commutation speed.

PACS numbers: 73.40.-c, 73.50. -h

The information age we live in is made possible by a physical underlayer of electronic hardware, which originates in condensed matter physics research. Despite the mighty progress made in recent decades, the demand for faster and power efficient devices continues to grow. Thus, there is urgent need to identify novel materials and physical mechanisms for future electronic device applications. In this context, transition metal oxides (TMOs) are capturing a great deal of attention for non-volatile memory applications [1]. In particular, TMO are associated to the phenomenon of resistive switching (RS) [2] and the memristor device [3] that is emerging as a competitive technology for next generation electronics [1, 4–10]. The RS effect is a large, rapid, non-volatile, and reversible change of the resistance, which may be used to encode logic information. In the simplest case one may associate high and low resistance values to binary states, but multi-bit memory cells are also possible [11, 12].

Typical systems where RS is observed are two-terminal capacitor-like devices, where the dielectric might be a TMO and the electrodes are ordinary metals. The phenomenon occurs in a strikingly large variety of systems. Ranging from simple binary compounds, such as NiO, TiO_2, ZnO, Ta_2O_5, HfO_2 and CuO, to more complex perovskite structures, such as superconducting cuprates and colossal magnetoresistive manganites [2, 4, 6, 9].

From a conceptual point of view, the main challenges for a non-volatile memory are: (i) to change its resistance within nano seconds (required for modern electronics applications), (ii) to be able to retain the state for years (i.e. non-volatile), and (iii) to reliably commute the state hundreds of thousands of times.

Through extensive experimental work in the past decade, a consensus has emerged around the notion that the change in resistance is due to migration of ionic species, including oxygen vacancies (V_O), across different regions of the device, affecting the local transport properties of the oxide. In particular, the important role of highly resistive interfaces, such as Schottky barriers, has also been pointed out [7, 9, 14].

In contrast with the experimental efforts, theoretical studies remain relatively scare. A few phenomenological models were proposed and numerically investigated, which captured different aspects of the observed effects [3, 13, 15, 16].

In this context gaining theoretical insight is of essence. Thus, in the present work we shall address one of the key aspects of the RS phenomenon, namely, the issue of the commutation speed of the resistance change. Our first striking result is a connection between the RS phenomenon and *shock wave* formation, a classic topic of non-linear dynamics [18]. In fact, we shall argue that the profile of oxygen vacancies that migrate during the resistive change forms a shock wave that propagates through the Schottky barrier and leaks onto the bulk of the device, which we schematically illustrate in Fig.1. We further validate the scenario by means of numerical simulations on a successful model of RS and by novel experiments done on a manganese based memristor device. Both model calculations and experiments reveal a striking scaling behaviour as predicted by the shock wave scenario.

Generalized Burgers' equation. When ions migrate through a *conducting* medium under the influence of strong applied voltage, they are likely to undergo a nonlinear diffusion process, as we explain in the following. The total ionic current $\mathbf{j}(t,\mathbf{x}) = \mathbf{j}_{diffusion} + \mathbf{j}_{drift}$ can be expressed as the sum of a diffusion current $\mathbf{j}_{diffusion} = -D\nabla u$ and a drift current $\mathbf{j}_{drift}$, which is induced by the local electric field $\mathbf{E}$ and the local concentration u. Together with the continuity equation $\partial_t u + \nabla \cdot \mathbf{j}(\mathbf{x},t) = 0$, this immediately gives us a generalized diffusion equation of the *Nernst–Planck type*. This would represent a linear driven diffusion equation, where the local electric field $\mathbf{E}$ to be held constant, i.e. independent of the local ion concentration u. In contrast, in (poorly) conducting media

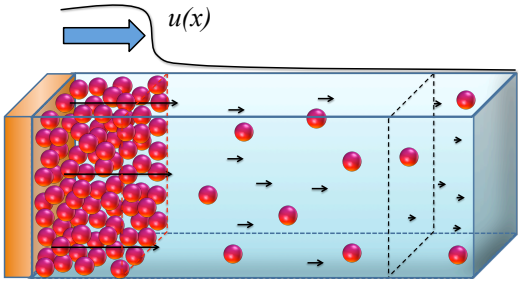

FIG. 1: Schematic representation of the shock wave evolution. The orange region indicates the metallic electrode and the blue indicates the TMO dielectric. Small spheres denote the ionic defects (oxygen vacancies) whose density profile form a shock wave. It evolves through a highly resistive (Schottky) interface and eventually leaks over the more conductive bulk, producing the resistive change. Black arrows depict the strength of the local electric fields.

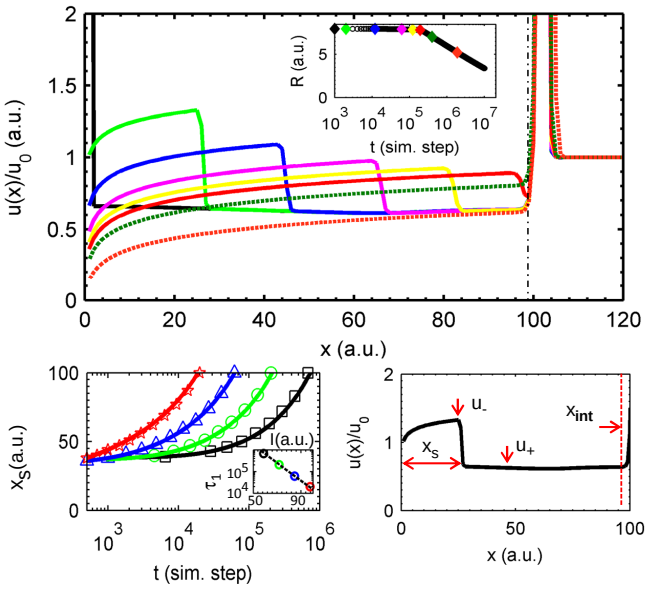

FIG. 2: Top panel: Snap shots of the time evolution of the $[V_O(x)]$=$u(x)$ profile within the active interfacial region in a simulation of the VEOVM (see Sup. Mat. for details). The current $I[a.u]$=11 and A_S=1000 and A_B=1. The time steps of the successive profiles can be read-off from the corresponding color dots in the inset. The initial state $u_0(x)$ (black line) exhibits a vacancy pile-up next to the electrode at x=1. The SB-B interface is denoted with a vertical dash-dot line at x_{int}=100. The large accumulation of vacancies on the right of x_{int} (bulk side) results from the initial "forming" cycles that conform an approximately fixed background [16]. Inset: Resistance of the device as a function of time. Color dots indicate the value of $R(t)$ at the corresponding snapshots of the main panel. Bottom-left panel: evolution of the shock wave front position $x_s(t)$ for different currents ($I[a.u]$=58.5, 71.5, 84.5 and 97.5). Dots are from numerical simulations and the solid lines are analytic fits from integration of Eq. (4). Inset: characteristic impact-time τ_1 as a function of applied currents from the numerical simulation (circles) and analytic fit (dotted-line) in semi-log scale. Bottom-right panel: Shock wave parameters.

and under voltage pulses, the local electric field may strongly depend on the local ion concentration; this effect is the key source of nonlinearity causing the formation of shock waves and very sudden resistance switching [7, 8].

Since electrons move much faster than the ions, we can view the ions as static when considering the electronic current $\mathbf{I}$, which obeys a steady-state condition $\nabla \cdot \mathbf{I} = 0$. The local electric field is then simply determined, through Ohm's law, by the local resistivity $\mathbf{E} = \rho(u)\mathbf{I}$, which may be a strong function of the local ion concentration u. In particular, in bad metals such as the transition metal oxides, the migrating ions (e.g. oxygen vacancies) act as scattering centers for the conduction electrons. In such situations, we expect $\rho(u)$ to be a *monotonically increasing* function of the local ion density $u(\mathbf{x},t)$. Therefore, the redistribution of the local ion density results in the change of local resistivities and, consequently, of the local electric fields, which further promotes the nonlinear effect in the drift.

Under the experimentally-relevant case where the transverse currents may be neglected, the problem simplifies to a one-dimensional non-linear diffusion equation,

$$\partial_t u + f(u)\,\partial_x u = D\partial_{xx} u, \qquad (1)$$

where $f(u) \equiv \partial_u j_{drift}(u,I)$, and $I(t)$ is the magnitude of the electronic current. Equation (1) can be considered a generalization of the famous *Burgers'* equation, which corresponds to the special case $f(u) \propto u$. Its most significant feature is the presence of a density-dependent drift term, *which physically means that the "crest of the wave" experiences a stronger external force than the "trough"*. This generally leads to the formation of a sharply defined *shock-wave* front in the u(x,t) profile, which assumes a universal form at long times, completely independent of the - quickly "forgotten" - initial conditions. Although the process is driven by the drift term, the stability of the shock wave form is provided by the existence of the diffusion term which prevents the shock wave from self-breaking[19, 23]. Remarkably, the formation of shock waves proves to be robust in a much more general family of models with the nonlinear drift term specified by the function $f(u)$, any *monotonically increasing* function of u. The qualitative behaviour can be established by using the well-known "method of characteristics"[19, 20], as we explain in more detail in the Supplementary Materials.

The drift current is generally given by the expression $j_{drift} = ug(E)$. The form of the function $g(E)$ is material-dependent, and here we envision two limiting situations. In homogeneous conductors, we should have simple "Ohmic" behaviour as $g(E) \sim E$ while in granular materials, we expect exponential dependence due to activated transport, corresponding to: $g(E) \sim \sinh(E/E_0)$, where E_0 is a parameter describing the activation process.

Remarkably, these general ideas find an explicit realization in the context of RS in transition metal oxide memristors, such

as manganites [14, 21]. In fact, their transport properties are very sensitively dependent on the oxygen stoichiometry, i.e. on the concentration of oxygen vacancies $[V_O]$. Thus, it is now widely accepted that the mechanism of the bipolar (i.e. polarity dependent) RS in those systems is due to the induced changes in the spatial distribution of $[V_O(\mathbf{x})] \equiv u(\mathbf{x})$ by means of externally applied strong electric stress [7, 8]. In particular, the accumulation of vacancies within highly resistive regions between the oxide and the metallic electrode, such as Schottky barrier (SB) interfaces, greatly increases the (two-terminal) resistance across the device [16]. This accumulation can be achieved by applying strong voltage pulses across the device, leading to the high resistance state R_{HI}. Abrupt resistance switching from such high-resistance state to a significantly lower resistance state can be accomplished by reversing the voltage applied, which removes a significant fraction of vacancies from the SB region. The precise characterization of this resistance switching process is the main subject of this paper.

We should mention that an important assumption is that the nonlinear drift term plays the dominant role as compared to the normal diffusion, i.e. we shall not be concerned with the resistive changes involving thermal effects [7, 8]. This restriction enables us to apply our analytical tools in a simple manner, allowing us to obtain a simplified mathematical description of the migration process, as we show in the following.

Model system. For concreteness, we adopt the *voltage-enhanced oxygen-vacancy migration model* [16] (VEOVM), which corresponds to granular materials with activated transport process and has been previously used for manganite devices [16]. Within the framework of this model, we shall perform numerical simulations to validate our shock-wave scenario. The VEOVM simply assumes that the local resistance of the cell at (discretized) position x along the conductive path of the device is simply given as a linear function of the local vacancy concentration, namely,

$$r(x) = A_\alpha u(x) \tag{2}$$

with $\alpha = S, B$, where S denotes the highly resistive (Schottky barrier) region and B the more conductive bulk [14]. The values of these constants are taken $A_S \gg A_B = 1$, which allows us to neglect the bulk resistance [16]. The discretized conducting assumes the metal-electrode at x=0 and $x = x_{int}$ denotes the point within the dielectric where the SB meets the bulk region. Under the action of the external stress (electric current I), the local fields at each cell position x are computed at every discrete time step t. The field-driven migration of vacancies is simulated computing the local ionic migration rates from cell x to $x+\Delta x$ as [16]

$$P(x, x+\Delta x) = u(x)[1-u(x)] \exp\left(\frac{-V_0 + qIr(x)}{k_B T}\right), \tag{3}$$

where, for simplicity, we take the ionic charge q=1 and $k_B T$=1. The parameter V_0 denotes the activation energy for ionic diffusion. The new profile $u(x,t)$ is updated from the migration rates, and from (2) we get the new total (two point) $R(t)$ as the discrete x-integral of the local cell's resistance $r(x,t)$. Here, for simplicity, we focus on a single active SB-bulk interface, while the more general situation with two barriers may be analyzed following a similar line of argument [16]. The applied external electric stress that we adopt is a constant current, in both, simulations and experiments (see below).

As described in Ref.16, the initial vacancy concentration profile is assumed to be constant $[u(x)] = [u^0]$. The "forming" or initialization of the memory is done by first applying a few current loops of alternative polarity, $\pm I^0$, until the migration of vacancies evolves towards a *limit cycle*, with a well defined profile $u_0(x)$. After this, the system begins to repetitively switch between two values: R_{HI} and R_{LO}. In the first, most of the vacancies reside within the high-resistance region SB, and in the second they accumulate vacancies in the more conductive bulk. The R_{HI} state with the vacancies piled up in the first cell, at x=1, defines the initial state for the shock wave propagation (see Fig.2).

Shock wave formation: the "propagation phase". We apply an external field with polarity pointing from the SB to the bulk and observe the evolution of the vacancy profile as a function of the (simulation) time. As can be observed in Fig.2 there is a rapid evolution of the profile into a shock wave form with a sharply defined front. We also notice that the total resistance remains approximately constant during an initial phase, and suddenly starts to decrease after the front hits the internal SB-bulk interface at x_{int} (inset of top panel of Fig.2). We shall analyze these key features in the following.

First, we focus on the propagation of the shock wave front position $x_s(t)$, as shown in Fig.2 (bottom-left panel) for different values of the electronic current I. We observe that the characteristic time τ_1 for the shock wave to travel through the Schottky barrier and reach the SB-bulk point x_{int} decreases exponentially with the magnitude of I. To obtain analytical insight for this behaviour, we recall that the velocity of the shock wave front dx_s/dt is very generally given by the Rankine–Hugoniot conditions [19, 22], which express it as the ratio of the spatial discontinuity of the (vacancy) drift current, and the spatial discontinuity of the density profile across the shock viz. $dx_s/dt = \Delta j/\Delta u|_{x_s}$. Within the VEOVM model [16], we obtain the following *nonlinear rate equation* (see Supplementary Materials for details), which describes the dynamics of the shock wave front:

$$\frac{dx_s}{dt} = \frac{2Du_- \sinh(IA_S u_-) - 2Du_+ \sinh(IA_S u_+)}{\Delta u}, \tag{4}$$

where D is a prefactor related to the activation energy for vacancy migration (Arrhenius factor) (see Eq.1 and Ref.16), and $u_{-/+}$ are the density of vacancies at the two sides of the shock wave front (see Fig.2). The density u_- depends on the shock wave front position via: $u_- = Q/x_s + u_+$, where Q is the total number of vacancies carried by the shockwave, which remains a constant parameter through the propagation phase ($t < \tau_1$) and u_+ is a constant background density which can be written as $u_+ = Q_B/x_{int}$, Q_B standing for the total number of background vacancies.

Our description of the propagation phase is fully consistent with our numerical simulations. As shown in the inset of Fig.2 (top panel), the resistance remains essentially constant until

the wave front reaches the SB-bulk interface after a (current dependent) time τ_1, and then begins to drop. Moreover, we also achieved a good fit to the shock front velocity by using Eq.4, as is shown in Fig.2 (see Sup. Mat. for details).

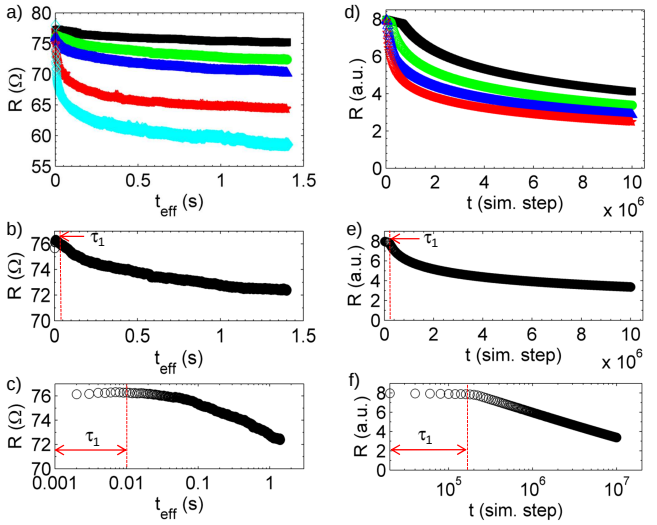

FIG. 3: Time dependence of the resistive change $R(t)$ for various external current intensities. Top left: experimental data measured on an Ag/LPCMO/Ag memristor with I = 37.5 mA (black), 40 mA (green), 50 mA (blue), 80 mA (red) and 100 mA (cyan). t_{eff} is the effective time duration of the applied currents (see Supplementary Material). The initial state was reset by applying an intense negative polarity current of 350 mA. Note that the initial value of the resistance, 78 Ω is recovered within ±1Ω. Top right: model simulations with applied current: $I[a.u.]$ = 58.5 (black), 71.5 (green), 84.5 (blue) and 97.5 (red). Middle panels: experimental data for I = 40 mA (left) and simulations for $I[a.u.]$ = 71.5 (right). τ_1 is defined as the time interval from the beginning of the applied pulse until the resistance starts to drop. Bottom panels: idem in a semi-log plot.

Resistance switching: the "leakage phase". After the shock front reaches the boundary point x_{int} the resistance begin to drop. To understand this behaviour, we note that the total resistance of the Schottky barrier is given by the *total number of vacancies* within the barrier region viz. from (2) $R_{SB} = \int_{SB} dx A_S u(x)$. As a result, the resistance drop per unit time is approximately given by the ionic vacancy-current passing through the SB-bulk interface at x_{int},

$$dR(t)/dt = -A_S j(x = x_{int}) \tag{5}$$

since $R_S \gg R_B$ as $A_S \gg A_B$. Notice that during the propagation phase the ionic current through the interface x_{int} is negligibly small. This is because the initial vacancy concentration there, and hence the local field, are also negligibly small. However, when the shock wave front eventually reaches the end of the SB region, after travelling for a time τ_1, we do expect a sudden resistance drop as a large number of ionic vacancies begin to leak out into the bulk region.

We shall now focus on the detailed description of the resistive drop. In Fig.3 we show the systematic dependence of $R(t)$ as a function of the applied external (electronic) current. Along with the simulations of the VEOVM, we also present our experimental results measured on a manganite-based ($La_{0.325}Pr_{0.300}Ca_{0.375}MnO_3$) memristive device. Experimental details are provided in the Supplemental Material. The set of curves were obtained for applied current intensities just above the threshold for the onset of the resistance switch. The goal was not to demonstrate the fast switching speed of the device, but rather on the contrary, achieve relatively slow switching speeds in order to access the different time scales. We observe that in both, simulation and experiments, the resistance change rapidly becomes larger and faster with the increase of the applied electric stress intensity. We also observe an overall good qualitative agreement between experiments and model simulations. This is also highlighted by the semi-log plots, which clearly display the two-stage process involved in the resistive switch, before and after the impact time τ_1.

Remarkably, within shock wave scenario, we may also obtain explicit expressions that quantify the resistance change during the leakage phase. Our analysis may be simplified by first noting, from general considerations of shock waves, that their shape at long times becomes "flat", i.e. the gradient of the local density rapidly decreases ($\partial_x u \to 0$) at all points that were overtaken by the shock wave front[19, 20]. Indeed, our data is fully consistent with this observation, as the vacancy density profile within the SB remains approximately "flat" (ie spatially constant $u(x,t) = u_S(t)$) at all times after the shock front reaches the interface (see Fig.2). Then, within the VEOVM the SB resistance is simply proportional to the total vacancy concentration within the barrier and we have, $R(t) \approx R_S(t) = A_S x_{int} u_S(t)$. Since the electronic current I is held fixed, the vacancy (i.e. ionic) current through the interface depends only on the vacancy concentration u_S (cf Eq.3). Thus, within the VEOVM we obtain a *nonlinear rate equation*, describing the resistance drop during the "leakage phase":

$$\frac{dR}{dt} = -\frac{2DR}{x_{int}} \sinh\left(\frac{IR}{x_{int}}\right). \tag{6}$$

Similarly as we showed before for the propagation phase, this equation may be validated by a quantitative fit to the simulation results (see Sup. Mat.). Note that due to the strong nonlinear form of this rate equation, the $R(t)$ response is significantly different from the simple exponential decay expected in the familiar linear case (e.g. in standard RC circuits). Therefore, within the short time scale associated with the initial fast drop of resistance and where the RS is significant ($IR/x_{int} \gg 1$), the present type of nonlinear system is dominated by the activated process and the approximation $\sinh(IR/x_{int}) \approx \frac{1}{2}\exp(IR/x_{int})$ is valid. This enables the approximate solution of the Eq.6.

$$R = R_{HI} - \frac{x_{int}}{I} \ln\left(1 + \frac{t}{\tau_2(I)}\right), \tag{7}$$

where the time is measured from the "impact" time τ_1 and $\tau_2(I) = \frac{x_{int}^2}{DIR_{HI}} \exp(-IR_{HI}/x_{int})$ (see Sup. Mat.) is the current-dependent characteristic time for the resistance drop.

Resistivity scaling. An interesting consequence of Eq.7 is that it suggests the scaling behaviour of the curves $R(t)$. In fact, one may define the normalized resistance drop $\delta R(t^*) =$

$R-R(\tau_2)/(R_{HI}-R(\tau_2))$ and see from Eq.7 that obeys it the scaling form:

$$\delta R(t^*) = 1 - \ln(1+t^*/\tau_2)/\ln(2), \qquad (8)$$

In Fig.4 we demonstrate that this striking feature is indeed present in both, our experiments and simulations data. In the upper panels of the figure we show the excellent scaling that is achieved, where all the experimental and the simulation curves $R(t)$ from Fig.3 were respectively collapsed onto a single one. Moreover, the collapsed data can also be fitted with a slightly more general form of Eq.8, that we discuss in the Supplemental Material. Remarkably, in the lower panels of Fig.4 we show that a collapse of the data $R(t)$ can also be obtained using the impact time τ_1 as the scaling variable. This is significant, because it shows that a single scaling behavior may include the two phases of the resistive switching process, namely before and after τ_1. We should mention that the scaling scenario was derived with the assumption of an ohmic behaviour in the *I-V* characteristics. While this may not be the case in general [17], within the present set of experiments, which are performed near the current threshold of RS, our results indicate that this is a reasonable assumption or at least a valid approximation.

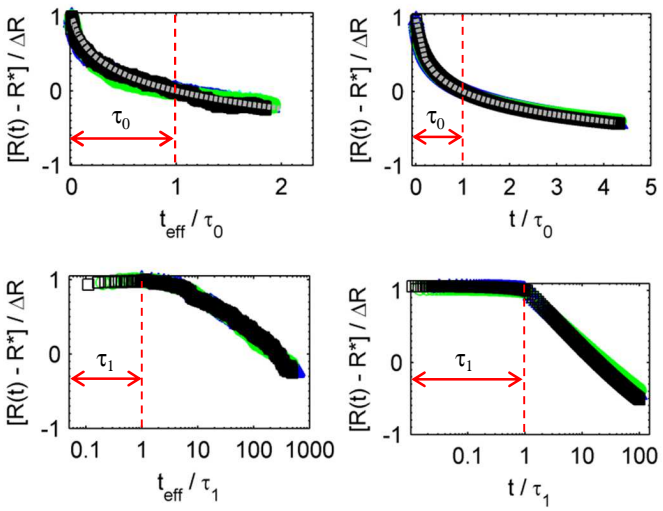

FIG. 4: Scaled curves of the $R(t)$ data sets of Fig.3. The left panels show the collapsed experimental data and the right ones the numerical simulations. The time τ_0 is an auxiliary scaling variable, which is proportional to the characteristic time τ_2 (see Sup. Mat. for details on the scaling procedure). The scaled data were fitted (white dotted line) with a generalized version of Eq.8 (see Sup. Mat.). The lower panels show the same data sets scaled with the shock wave impact time τ_1 (the experimental curves show only three data sets for the lower current values. At higher currents our electronics could not resolve τ_1). To achieve the scaling of the lower panels, we assumed for each plot the normalization value of ΔR determined from the previous scaling (top panels).

To conclude, from quite general considerations of migration of ionic defects under strong electric fields in solids, we have argued that the dynamics of the spatial profile of defect concentration should be governed by a Burgers'-type nonlinear equation and develop shock waves. We demonstrated that this scenario is indeed realized within a concrete realization, namely a ionic migration model that was previously applied to describe resistive switching phenomena in manganite based memristive devices. In those systems, a key role is played by the migration of oxygen vacancies, which are the ionic defects relevant to the electronic transport properties. We thus predicted a two-stage process for the resistive switch phenomenon. An initial one, where the oxygen-vacancy concentration profile develops a shock wave that propagates throughout a highly resistive (Schottky barrier) region near the electrode. During this phase the resistance essentially does not change. This is followed by a second phase, where the shock wave emerges from the high resistive region and the ionic defects leak into the conductive bulk. Our scenario was further validated by novel experimental data on a manganite based memristor device. A remarkable results of our study is that both, the numerical simulations and the experimental curves, obeyed a scaling behaviour, providing decisive support to our theory. The present work provides novel insights on the physical mechanism behind the commutation speed on novel nonvolatile electronic memories, unveiling an unexpected connection between a phenomenon of technological relevance and a classic theme of nonlinear dynamical systems.

This work was partially supported by public grants from the French National Research Agency (ANR), project LACUNES No ANR-13-BS04-0006-01, the NSF DMR-1005751and DMR-1410132, the University of Buenos Aires (UBACyT 2013-2016) and the Conicet PIP-2013-MeMO.

[1] International technology road map for semiconductors http://www.itrs.net/, (2011).

[2] M.J. Rozenberg, Scholarpedia, 6, 11414, (20011),

http://dx.doi.org/10.4249/scholarpedia.11414.
[3] D.B. Strukov, G.S. Snider, D.R. Stewart, and R.S. Williams, Nature, 453, 80-83 (2008).
[4] R. Waser , M. Aono , Nat. Mater. **6** , 833 (2007).
[5] J.J. Yang, M.D. Pickett, X. Li, D.A.A. Ohlberg, D.R. Stewart, and R.S. Williams, Nature Nanotechnol., 3, 429-433 (2008).
[6] R. Waser, R. Dittmann, G. Staikov, and K. Szot, Advanced Materials, 21,6, 2632-2663 (2009).
[7] I.H. Inoue and A. Sawa, Chapter 16 of a book "Functional Metal Oxides, New Science and Novel Applications": Wiley-VCH, Germany (Eds. Ogale S, Venkatesan T, Blamire M)(2013).
[8] J.J. Yang, I.H. Inoue, T. Mikolajick, C.S. Hwang. MRS bulletin **37** (02), 131-137, (2012).
[9] A. Sawa, Materials Today, 11, 28-36 (2008).
[10] A. Baikalov, Y.Q. Wang, et. al, App. Phys. Lett., 83,5, 957 - 959 (2003).
[11] P. Stoliar, P. Levy, M.J. Sánchez, A.G. Leyba, A.C. Albornoz, F. Gomez-Marlasca, A. Zanini, C. Toro Salazar, N. Ghenzi, M.J. Rozenberg, IEEE TRANSACTIONS ON CIRCUITS AND SYSTEMS II: EXPRESS BRIEFS, 61,1, 21 - 25 (2014).
[12] F. Alibart, L. Gao, B. D. Hoskins, and D. B. Strukov, Nanotechnology, **23**, no. 7, p. 075201 (2012).
[13] M.J Rozenberg, I.H. Inoue, and M.J. Sanchez, Phys. Rev. Lett., 92,17, 178302 (2004).
[14] X. Chen, N. J. Wu, J. Strozier, and A. Ignatiev, Appl. Phys. Lett. **87**, 233506 (2005).
[15] Russo, U.; Ielmini, D.; Cagli, C.; Lacaita, AL., "Filament Conduction and Reset Mechanism in NiO-Based Resistive-Switching Memory (RRAM) Devices," Electron Devices, IEEE Transactions on , vol.56, no.2, pp.186,192, Feb. 2009
[16] M.J Rozenberg, M.J. Sanchez, R. Weht, C. Acha, F. Gomez-Marlasca, and P. Levy, Phys. Rev. B, 81, 115101 (2010).
[17] F. Gomez-Marlasca, N. Ghenzi, A.G. Leyba, A.C. Albornoz, D. Rubi, P. Stoliar, and P. Levy, J. Appl. Phys., 113, 144510 (2013).
[18] Introduction To Fluid Mechanics Fourth Edition, Robert W. Fox, Alan T. McDonald ISBN 0-471-54852-9
[19] L. Debnath, *Nonlinear partial differential equations for scientists and engineers* (Birkhauser, 2011).
[20] R. Courant and D. Hilbert, *Methods of mathematical physics. Vol. II: Partial differential equations* (Interscience, New York, 1962).
[21] H-S Lee, S-G Choi, H-H Park and M. J. Rozenberg; Scientific reports **3**, 17 (2013).
[22] E. L. LD Landau, *Fluid Mechanics: Volume 6 (Course Of Theoretical Physics)* (Butterworth-Heinemann, 1987).
[23] M. Taylor, Applied Mathematical Sciences (2011).

Supplemental Material for Shock-waves and commutation speed of memristors

Shao Tang,[1] Federico Tesler,[2] Fernando Gomez Marlasca,[3] Pablo Levy,[3] V. Dobrosavljević,[1] and Marcelo Rozenberg[4]

[1]*Department of Physics and National High Magnetic Field Laboratory, Florida State University, Tallahassee, FL 32306, USA*

[2]*Departamento de Física - IFIBA, FCEN, Universidad de Buenos Aires, Ciudad Universitaria Pabellón I, (1428) Buenos Aires, Argentina*

[3]*GIA-CAC - CNEA, Av. Gral Paz 1499 (1650) San Martín, Pcia Buenos Aires, Argentina.*

[4]*Laboratoire de Physique des Solides, CNRS-UMR8502, Université de Paris-Sud, Orsay 91405, France*

PACS numbers: 73.40.-c, 73.50. -h

arXiv:1411.4198v3 [cond-mat.mtrl-sci] 18 Mar 2016

I. METHOD OF CHARACTERISTICS

In this section, we demonstrate that shock wave are formed in general as a consequence of the nonlinearity. We analyze the problem under generic circumstances via the *method of characteristics*. We then provide an explicit example which is qualitatively different from the situations discussed in main text.

Considering the vacancy migration in high resistive barriers where we can neglect the normal diffusion term $D\partial_{xx}u$, we would then obtain that the first order, quasi-linear partial differential equation has the form $a(u,t,x)\partial_t u + c(u,t,x)\partial_x u = b(u,t,x)$ in general and the u dependence in $c(u)$ is responsible for the onset of the shock wave. The characteristics[1, 2] are defined as (using s as a parameter along these curves):

$$\begin{cases} \frac{dt}{ds} = a(u,t,x) \\ \frac{dx}{ds} = c(u,t,x) \\ \frac{du}{ds} = b(u,t,x) \end{cases} \tag{1}$$

We have the following equation as the ion's motion in barrier is concerned:

$$\partial_t u + c(u,t)\partial_x u = 0 \tag{2}$$

We can immediately write down the characteristic equations which are simply $du/dt = 0$ and $dx/dt = c(u,t)$ with $dt/ds = 1$. It's easy to see that u is a constant along the characteristics since $du/dt = dx/dt\,\partial_x u + \partial_t u = 0$. Starting from the initial data, different lines might intersect with each other, indicating different values of $u(t = 0,x)$ which propagates from initial position meet each other hence the u at this point on $t - x$ plane is multi-valued. The intersection which happens first chronologically determines the onset of the shock wave as shown in Fig.S1.

We would elaborate in a more physical way as follows with the nonlinear drift term which satisfies the condition $\partial_u c(u,t) > 0$. Considering (2) as a simple wave equation, it's obvious that a travelling wave with speed locally proportional to c is the solution. (Compared to a more basic situation where $c(u,t)$ is independent of u, then we obtain a travelling wave with the same speed for every point.) Consequently, the characteristics defined above records the path as every point with a definite u moves in $t - x$ plane. Therefore, at any given time, spatially different points move with the different speed proportional to $c(u,t)$ and the "crest" with the largest value of u move fastest which leads to a "kink" type shock. It's also straightforward to check that if $\partial_u c(u,t) \leq 0$, there would be no shock with steep wave front formed. In the case where $c(u,t)$ is independent of u, the characteristics are curves with completely the same shape, paralleling to each other and hence would not have any intersections. Considering the polarity with drift force pointing from left barrier to conductive bulk, as long as the initial data $u(t = 0,x)$ is *not everywhere non-decreasing* (there exists two points $x_1 < x_2$ with initial data satisfies $u(t = 0,x_1) > u(t = 0,x_2)$), the shock wave would be established after some time since $\partial_u c(u,t) > 0$.

Therefore, upon reversing the polarity, most of the vacancies accumulates in the left end of the barrier with $u(t = 0,x)$ to be a strong decreasing function, experiencing the significant drift force pointing to the conductive bulk which guarantees the quick onset of the shock wave front (kink) with relative large amplitude.

As an illustration, we provide an example with $c(u,t) = u^2$ and the Gaussian distributed initial data as $0.5\exp\left[(x-5)^2/4\right]$. The time dependent wave profile is solved numerically with fixed boundary condition with characteristics computed according to Eq.1.

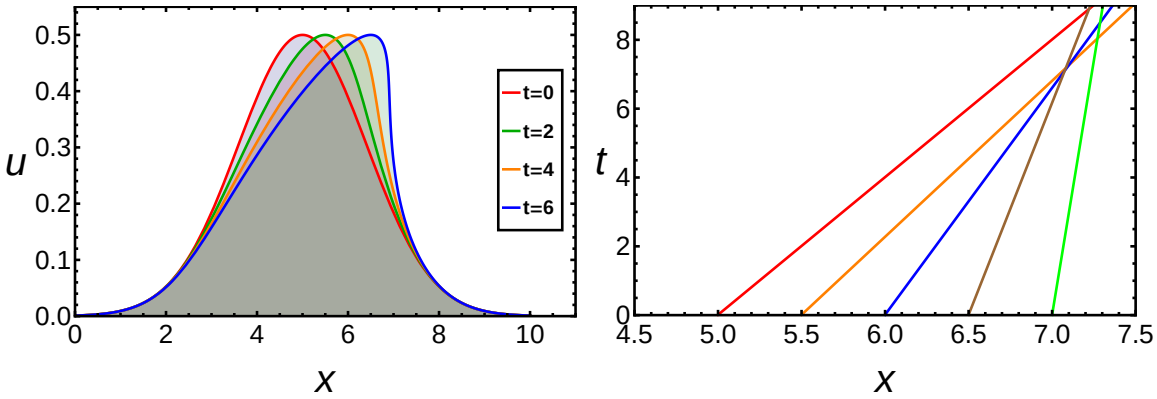

Figure 1: Left panel: The motion of the wave and the shock with steep wave front forms at $t = 6$ approximately. Right panel: Corresponding characteristics start at $x_0 = 5, 5.5, 6, 6.5, 7$ separately and crosses happen around $t = 6$, indicating the onset of shock wave.

II. DYNAMICS OF SHOCK WAVE

In this section, we provide a simple derivation of the Rankine–Hugoniot conditions[1, 3] which determines the equation of motion of the shock wave front. Notice that an important feature of the shock is the spatial discontinuity of u and also j. Considering a shock wave front propagating between the interval $[0,d]$ in 1D, we then define $u_+ \equiv u(t, x_s(t)+\varepsilon)$, $u_- \equiv u(t, x_s(t)-\varepsilon)$, $j_+ \equiv j(t, x_s(t)+\varepsilon)$ and $j_- \equiv j(t, x_s(t)-\varepsilon)$ correspondingly with $x_s(t)$ to be the coordinate of the shock wave front and $\varepsilon \to 0^+$ is a infinitesimal positive quantity. According to the continuity equation $\partial_t u + \partial_x j = 0$, we have:

$$\frac{d}{dt}\left(\int_0^{x_s(t)} u dx + \int_{x_s(t)}^{d} u dx\right) = j(0) - j(d) \tag{3}$$

$$\frac{dx_s}{dt}u_- - \frac{dx_s}{dt}u_+ + \int_0^{x_s(t)} \partial_t u dx + \int_{x_s(t)}^{d} \partial_t u dx \;=\; j(0) - j(d) \tag{4}$$

Applying the continuity equation again, we obtain the shock wave velocity as follows:

$$v_s = \frac{dx_s}{dt} = \frac{j_+ - j_-}{u_+ - u_-} = \frac{\Delta j}{\Delta u}|_{x_s} \tag{5}$$

Therefore, we obtain the equation of motion regarding the shock wave front which is valid for a general form of $j(u,t,x)$.

III. VEOVM MODEL

As it was mentioned in the main text, to simulate the vacancies dynamics we adopted *the voltage enhanced oxygen vacancy migration model* (VEOVM), which is a well validated model for the RS effect. Taking a capacitor-like device, this model considers a 1 dimensional conductive channel connecting the two contacts, along which oxygen vacancies can migrate through (see Fig.S2). This channel is divided in small cells corresponding to physical nano-domains, and at the same time the whole device is divided in two regions: the active interfacial region close to the metal contact (i.e. high resistive Schottky Barrier) and the high conductive bulk region. A diagram of the model with a single active contact, as used in the simulations, is presented at the top panel on Fig.2. The resistance of each cell in the channel $r(x)$ is proportional to the local density of vacancies: $r(x) = u(x)A_\alpha$, where $u(x)$ is the density of vacancies on the cell located at x and A_α is a proportionality constant whose magnitude depends on the region of the device: $\alpha = S, B$, where S stands for Schottky barrier and B for bulk, and where $A_s \gg A_B$. Migration is assumed to occur only between neighbours cells, and in each step of the simulation the probability for vacancy migration from a cell at x to its neighbour at $x + \Delta x$ is computed according to:

$$P(x, x+\Delta x) = u(x)(1 - u(x+\Delta x))\exp(\Delta V(x) - V_0), \tag{6}$$

where $\Delta V(x)$ is the drop of voltage (per unit length) at x and V_0 is an activation constant for vacancy migration. In each step of the simulation the migration from cell to cell is computed and the new resistance of each cell is calculated. The total resistance of the device is calculated simply as the addition of all the cells in the channel. For the values of used in the simulations, the middle term $(1-u(x+\Delta x))$ can and will be neglected in the theoretical analysis explained in the following sections. As mentioned in the main text, this model corresponds to the case of granular materials with activated transport process. To put it in the context of the $generalized-Burgers'equation$ description made in main text, it is easy to see that the drift current originated from this model satisfies the general form $j_{drift} \sim \sinh(E)$. The net current of vacancies generated by the action of an external electric field $E(x) = \partial V(x)/\partial x$, between a cell at x and its neighbour cell at $x+\Delta x$ can be written simply as Fick's-law for the migration probability: $j_{drift} = \partial P/\partial x \approx [P(x,x+\Delta x) - P(x+\Delta x,x))]/\Delta x$, where in the last term the discrete character of the model has been introduced. In particular for our model we take $\Delta x = 1$. Using the definition of P from the model (neglecting its middle term), we get from here that $j_{drift} = P(x,x+\Delta x) - P(x+\Delta x,x) = 2Du\sinh(\Delta V(x))$, where D stands for the Arrhenius factor $\exp(-V_0)$. If the external electric stress is a controlled current I, then $\Delta V(x) = Ir(x) = IA_\alpha u(x)$.

IV. SIMULATIONS DETAILS

In order to analyze the existence of a shock wave scenario, the Hi to Lo process was simulated for different external currents. Previously, an initial forming process was performed at which current of different polarities was applied and well defined Hi and Lo states were obtained. In the bottom panel on Fig.2 the vacancy profile is shown before and after the forming process. The device starts with a uniform distribution along the channel, and by the end of the forming process the profile shows a characteristic distribution in which vacancies that were originally in the interfacial region migrates to the low-field bulk region where they are accumulated. The figure shows the formed Hi resistance state where it can be seen a second accumulation of vacancies next to the left metal contact in the interfacial region. This second accumulation of vacancies conforms the initial distribution for the Hi to Lo process and it will evolve to form the shock wave during switching as shown in the main text. To improve the stability of the simulations the currents were applied using a rise time (from 0 to their actual values) always negligible compared with the characteristic times of the process τ_1 and τ_2 (with rise times in the order of a few thousands of steps). The simulated device contained a total of 1000 cells with a 100 cells long interfacial region (left interface). For the initial distribution a uniform density of $u_0 = 1\times 10^4$ per cell was used. The value of the activation constant V_0 was set to 16, and for the resistivity constants we used $A_S = 1000$ and $A_B = 1$.

V. FITTING FOR VEOVM MODEL

In this section, we explain the details of the comparison between simulation and theory and the procedures used for fitting. Consider the drift current within left interfacial region in VEOVM model:

$$j(u,t,x) = P(x,x+\Delta x) - P(x+\Delta x,x) = 2Du\sinh(IA_S u) \tag{7}$$

where the term $1-u(x+\Delta x)$ in the probability has been neglected as explained before [7]. From Eq. (9) we have, as shown in the main text:

$$\frac{dx_s}{dt} = \frac{2Du_-\sinh(IA_S u_-) - 2Du_+\sinh(IA_S u_+)}{\Delta u}, \tag{8}$$

where x_s is the shock wave front position, u_- is the density of vacancies inside the shockwave (assumed uniform), u_+ is the density outside the shockwave (background vacancies), I is the applied current, and D is the Arrhenius factor $\exp(-V_0)$.

Performing a redefinition of parameters (for practical reasons only) we can rewrite the last equation as:

$$\frac{dx}{dt} = \frac{2D}{x_{int}}\left[\left(1+\frac{\alpha}{\beta}x\right)\sinh\left(\frac{I}{\beta}+\frac{I}{\alpha x}\right) - \frac{\alpha}{\beta}x\sinh\left(\frac{I}{\beta}\right)\right], \tag{9}$$

where we used that $u_- = u_+ + \Delta u$, $Q = \Delta u x_s$ is the total number of vacancies carried by shock wave, $Q_B \equiv u_+ x_{int}$ is total number of background of vacancies in the left region (being x_{int} the length of the interfacial region), $x \equiv x_s/x_{int}$ is the normalized coordinate, and where we defined the new parameters $\alpha \equiv x_{int}/A_S Q$ and $\beta \equiv x_{int}/A_S Q_B$. From the previous definitions we can write the high resistance value as $R_{HI} = A_S(Q_B+Q)$ where R_{HI} is a constant determined by the vacancy concentration and independent of I [8].

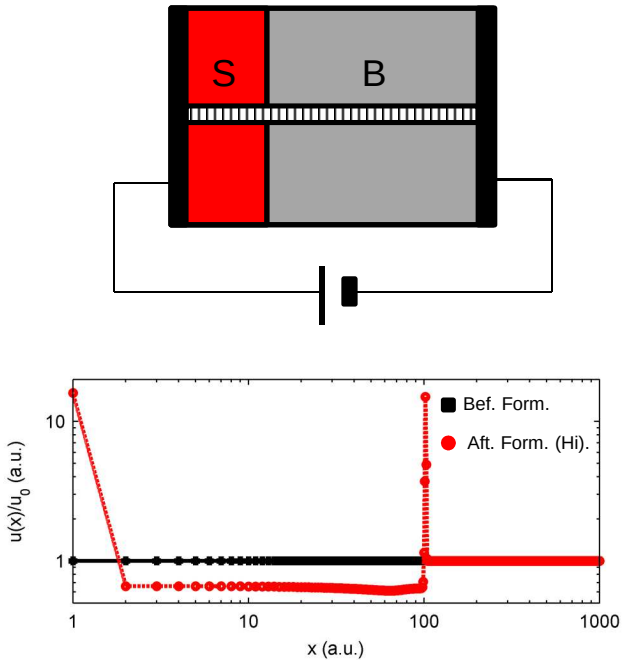

Figure 2: Top panel: Schematic diagram of the VEOVM model with a single active contact. The two regions S and B correspond to the high resistance interface (Schottky Barrier) and the more conductive central bulk, respectively. The small cells within the channel indicate the domains. Bottom panel: vacancy distribution along the conductive channel before (black squares) and after (red circles) the forming process. The distribution shown after the forming process correspond to a Hi resistance state. Starting from a uniform distribution, during the forming process a characteristic distribution is obtained where vacancies initially at the interface migrates to the low-field bulk region generating a pile-up of vacancies close to the limit between the two regions. In the Hi state, part of these vacancies migrates back to the interfacial region and are accumulated in the vicinity of to the metal contact.

We can solve then this equation numerically with the material dependent parameters x_{int}, α,β and D. Considering the initial rise time for the current and the non-flatness of the shock wave, an accurate test of the $x_s(t)$ prediction can be performed for $x > x_0 \approx 0.4$ using the integral-form equation:

$$t - t_0 = \int_{x_0}^{x} \frac{(x_{int}/D)\,dy}{2\left(1+\frac{\alpha}{\beta}y\right)\sinh\left(\frac{I}{\beta}+\frac{I}{\alpha y}\right) - \frac{2\alpha}{\beta}y\sinh\left(\frac{I}{\beta}\right)} \tag{10}$$

which is used for the fit of the simulation data for $t < \tau_1$ in the lower left panel of Fig.1 in the main text.

On the other hand, we have also the rate equation for the switching (i.e. "leakage") phase (cf. Eq.4 from main text):

$$\frac{dR}{dt} = -\frac{2DR}{x_{int}}\sinh\left(\frac{IR}{x_{int}}\right) \tag{11}$$

The numerical solution of this equation is used to fit the simulation data in the resistance switching phase for $\tau_1 < t$, shown in Fig.S3.

The values of the parameters that enter the equations (10) and (11) were extracted directly from the simulation results (Fig.1 of main text). We find $Q_B = 63.4u_0$, $Q = 15.3u_0$, $A_S = 1000$, $R_{HI} = 7.9a.u.$ and $D = 1.12 \times 10^{-7}$. The very good fits of the simulation data shown in Fig.1 and Fig.S3 were achieved by slightly relaxing the value of the single parameter x_{int}=100 to the values 94.3 (Fig.1) in the propagation phase and 82.2 (Fig.S3) in the leakage phase.

The small discrepancy between the relaxed parameters and its actual value mainly comes from the non-flatness of the density profile both during the propagation of the shock wave and during the leaking phase, as well as from the fact that a small part of background vacancies leaks into the bulk during the propagating phase.

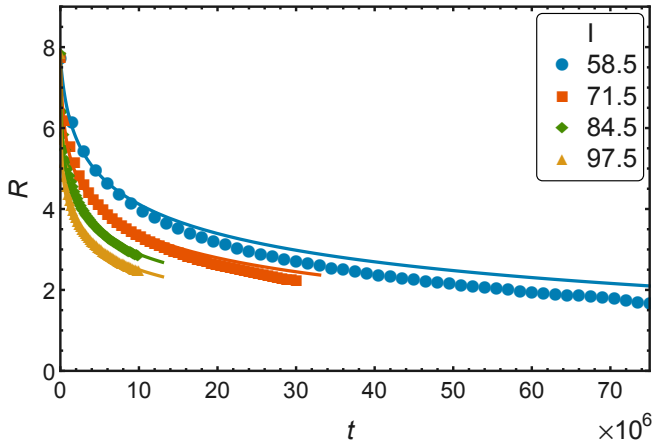

Figure 3: Evolution of the resistance during the switching phase for different applied currents according to simulations (dots) and theory (lines) from Eq. (11). The currents shown are $I = 58.5a.u., 71.5a.u., 84.5a.u.$ and $97.5a.u.$

VI. SCALING

In this section, we show that the scaling behaviour is a direct consequence of the strong non-linearity of the drift current $j(u,t,x)$, which depends on local electric field exponentially. In the time range where significant resistive switching occurs, we have $(IR/x_{int} \gg 1)$ and we may approximate $\sinh(IR/x_{int}) \approx \frac{1}{2}\exp(IR/x_{int})$. From Eq.(11), using a normalized resistance $\widetilde{R} = R/R_{HI}$, we have:

$$\frac{d\widetilde{R}}{dt} = -\frac{D}{x_{int}}\exp\left[\left(\frac{IR_{HI}\widetilde{R}}{x_{int}}\right)(1+\lambda)\right], \tag{12}$$

where $\lambda = \frac{x_{int}}{R_{HI}}\ln\widetilde{R}/\left(I\widetilde{R}\right)$ is a small parameter as long as $\widetilde{R}$ close is to 1 (i.e. at the beginning of the resistive change). For simplicity we consider the leading order as we set $\lambda = 0$:

$$\widetilde{R} = 1 - \frac{x_{int}}{IR_{HI}}\ln\left(1+\frac{t^*}{\tau_2}\right), \tag{13}$$

where $t^* = t - \tau_1$ is the time measured from the impact time as explained in main text, and τ_2 is a characteristic time for the resistance switch and is dominated by an exponential dependence of the applied current as follows:

$$\tau_2 = \frac{x_{int}^2}{DIR_{HI}}\exp\left(-\frac{IR_{HI}}{x_{int}}\right). \tag{14}$$

In Fig.S4 we use this approximate expression to fit the $R(t)$ simulation data. Comparison with the previous fit done with Eq.11 and shown in Fig.S3 allows us to check that this approximate solution is relatively accurate within the time domain we are interested in for fast switching devices.

Now, using Eq. (13), we can show that the I-dependent family curves $R(t)$ should obey scaling. We first consider the normalized resistive change $\delta R(t)$ defined as

$$\delta R(t) = \frac{R(t) - R(\tau_0)}{R_{HI} - R(\tau_0)} \tag{15}$$

where τ_0 is some yet unspecified time (and we drop the $*$ from t^*). Then, replacing with Eq.13 we have,

$$\delta R(t) = \frac{R_{HI} - \frac{x_{int}}{I}\ln(1+\frac{t}{\tau_2}) - R_{HI} + \frac{x_{int}}{I}\ln(1+\frac{\tau_0}{\tau_2})}{R_{HI} - R_{HI} + \frac{x_{int}}{I}\ln(1+\frac{\tau_0}{\tau_2})} \tag{16}$$

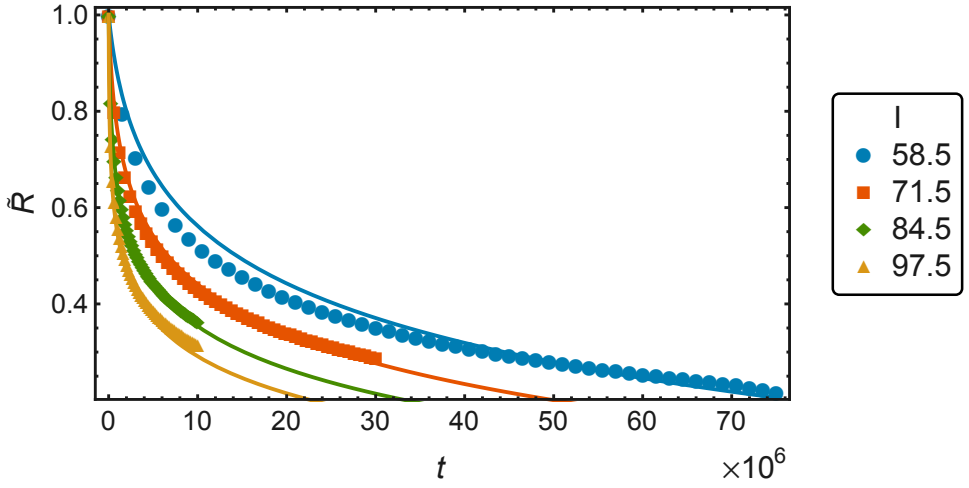

Figure 4: Fitting results for the evolution of the normalized resistance according to the Eq. (13).

And rescaling the time by τ_0,

$$\delta R(t/\tau_0) \;=\; 1-\frac{\ln(1+\frac{\tau_0}{\tau_2}\frac{t}{\tau_0})}{\ln(1+\frac{\tau_0}{\tau_2})} \tag{17}$$

Notice that with the natural choice of simply setting τ_0 as τ_2, we obtain the scaling form that we presented in the main text.

However, in the experiment we do not know, a priori, how to determine the characteristic time scale τ_2, which is a strong function of the current I and other material parameters. So we adopt the following strategy. We use τ_0 as a free scaling parameter, one for each I-dependent curve $R(t)$, that we rescale according to Eq.17. We vary the set of values $\tau_0[I]$ until we obtain a collapse of all the experimental and the simulation curves. The results of the successful collapse are shown in Fig.4 of the main text. In our experience, the collapse is unique. A crucial point now is that the collapsed set of curves could be fitted with the expression

$$F(t) = 1-\frac{\ln(1+ct)}{\ln(1+c)}. \tag{18}$$

with c a *current independent* constant. We find the values $c = 15.2$ for the experimental data and $c = 29.4$ for the simulation ones. Hence, in regard of Eqs.17 and 18 we observe that the constant c is nothing but the ratio between the analytically established characteristic time τ_2 and the empirically determined τ_0, which are simply proportional to one another.

In Fig.S5 we plot the dependence of the scaling time as a function of the applied current $\tau_0(I)$. In the case of the simulation results, the data follow the same exponentially decreasing behaviour as deduced for $\tau_2(I)$ (see Eq.14). Moreover, we find the ratio $\tau_0(I)/\tau_2(I)$ in good agreement with the constant $c = 29.4$, which validates our practical scaling procedure for the determination of the characteristic switching time in the experimental case.

Under the same set of approximations that we have assumed in this section, plus the additional one of neglecting the effect of the background distribution of vacancies, one may also derive an explicit expression for the characteristic time τ_1. We start from Eq. (9), and similarly as before, adopt the approximation $\sinh(IR/x_{int}) \approx \frac{1}{2}\exp(IR/x_{int})$. Then, making the substitution $y' = 1/y$ in Eq. (10), and assuming that the integral is dominated by the exponential factor (i.e. neglecting the change in lower order factors), the integral has an analytical solution, and we get for the case with no background vacancies (i.e. $1/\beta = 0$)

$$\tau_1 \approx C(t_0,x_0) + \frac{x_{int}^2}{DIR_{HI}}\exp\left(-\frac{IR_{HI}}{x_{int}}\right). \tag{19}$$

where the first term is the integration constant determined by the initial conditions t_0 and x_0. If this constant can be neglected (for example for fast forming shock waves) then we have the surprising result that $\tau_1 = \tau_2$.

In the case of the model simulations, the results displayed in Fig.S5 shows that, in fact, both characteristic times have the same I-dependent exponentially decaying behaviour. Moreover, the ratio of the two characteristic times is approximately 25, which is close to the constant $c = 29.4$ quoted before, therefore our simulations also validate the equality between the two characteristic times τ_1 and τ_2 predicted by the shock wave scenario.

As may be expected, the experimental situation is only qualitatively consistent with the previous discussion. As seen in Fig.S5, for the experimentally determined characteristic times, we observe that they have approximately a similar dependence with the applied current, however, it is less clear if the equality between them also holds.

We show and compare the evolution of both characteristic times under different applied current in Fig.S5 for both simulations and experiments, observing a good agreement with the analysis presented here.

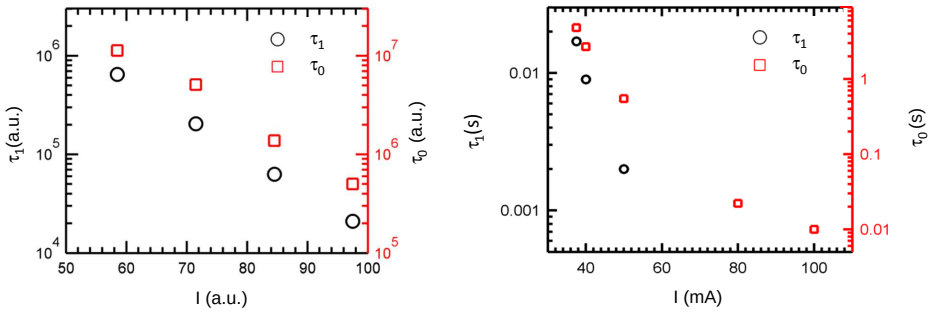

Figure 5: Evolution of the characteristic times for different applied currents for both simulations (left panel) and experiments (right panel). It can be seen that both times follow an approximate exponential dependence with I, and that there exist a relative proportionality between them as predicted by our analysis.

VII. EXPERIMENTAL DETAILS

For the experimental validation of our theory, the RS phenomenon was studied in a bulk $La_{0.325}Pr_{0.300}Ca_{0.375}MnO_3$ (LPCMO) polycrystallline sample with hand painted mm seized Ag contacts.

To induce the RS effect an external constant current was used as the electric stimulus. To generate this current and to acquire the data a Keithley 2612 Sourcemeter was employed. The measurements were done using a 3 wire configuration in order to measure a single interface resistance (Fig. 6.a). The Hi to Lo RS was studied for currents of different magnitude, as described in the main text.

The application of current is done following a pulsed protocol: a high current pulse (Write) is followed by a low current pulse (Read). A schematic diagram of the pulsed protocol is shown in (Fig. 6.b. Each pulse lasts 1ms. Between two pulses there is an interval of about 0.5s, meant to reduce possible heating effects. The time axis exhibited in the R vs t curves (both in Fig. 3 in the main text, and in Fig. 6.c, below) is the effective time elapsed during the actual application of the Write pulses, i.e. disregarding both the 0.5 s timeout and the Reading elapsed time. The Write pulses possess enough strength to change the resistive state of the system, while the Read pulse (low current) measures the remnant (stable, non-volatile) resistance of the device without affecting it. In the experiments shown in main text, the Write pulses are in the order of the mA while the Read pulses are in the order of the μA.

The complete measurement process is shown in Fig. 6.c. To obtain the initial Hi state, pulses of -350mA were applied (Fig. 6.c, left panel). Next, the desired accumulation experiment is performed, by applying positive pulses of constant amplitude which decrease the resistance (Fig. 6.c, middle panel). The initial Hi -resistance state is recovered by applying -350 mA pulses (Fig. 6.c, right panel). In every case the initial Hi-resistance state obtained was of the same magnitude within a range of about 1%.

[1] L. Debnath, *Nonlinear partial differential equations for scientists and engineers* (Birkhauser, 2011).
[2] R. Courant and D. Hilbert, *Methods of mathematical physics. Vol. II: Partial differential equations* (Interscience, New York, 1962).
[3] E. L. LD Landau, *Fluid Mechanics: Volume 6 (Course Of Theoretical Physics)* (Butterworth-Heinemann, 1987).
[4] A. Sawa, Materials Today, 11, 28 (2008).
[5] Y.B. Nian, J. Strozier, N.J. Wu, X. Chen, and A. Ignatiev, Phys. Rev. Lett., 98, 146403 (2007).
[6] E. Dagotto, T. Hotta, and A. Moreo, Physics Reports, 344, 1(2001).
[7] The typical value of $u(x)$ in simulation varies between 10^{-4} and 10^{-3}.
[8] There is in fact a small migration of background vacancies into the bulk during the period of shockwave propagation which causes a small variation of the resistance during this phase.

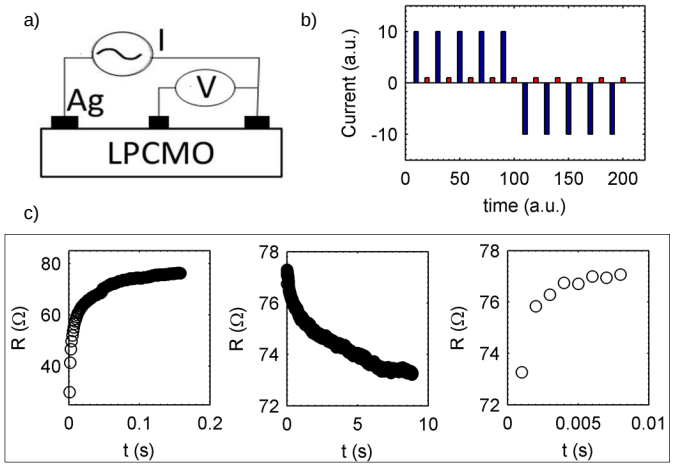

Figure 6: (a) Diagram of the experimental set up. (b) Sketch of the pulsed current protocol used in the experiments. A hight current Write pulse (blue) is followed by a low current Read pulse (red). The first pulse generates the RS while the second pulse measures the non-volatile resistance. (c) Rvst curves from a complete RS process. The system is first taken to a Hi resistance state under a current of -350mA (left panel). Then the Hi to Lo RS is measured under an applied current of 37.5mA (middle panel). Finally the system is taken back to a Hi resistance state with the application of a -350mA current.